Seismic Design of the Mercado Santa Anita Station in L2 Metro Lima Project

Julio RODRÍGUEZ-SÁNCHEZ
MSc. Civil Engineer, Ph.D. Candidate
AYESA Ingeniería y Arquitectura
Junior Engineer
jrsanchez@ayesa.com

Antonio Jesús DÍAZ-MORENO
MSc. Mechanical Engineer
AYESA Ingeniería y Arquitectura
Structural Engineering Advisor
adiazmoreno@ayesa.com

Guillermo MARTÍNEZ-RUIZ
MSc. Geological Sciences
AYESA Ingeniería y Arquitectura
Chief of Geotechnical Department
gmartinez@ayesa.com

Ignacio HINOJOSA SÁNCHEZ-BARBUDO
Ph.D. Civil Engineering, Associate Professor at University of Seville
AYESA Ingeniería y Arquitectura
CEO Engineering in Spain
ihinojosa@ayesa.com

ABSTRACT

Underground structures are the main part of crucial infrastructures in cities, and should withstand severe earthquakes without any loss of capacity. L2 of Metro Lima is the most ambitious underground transportation facility that is planned in South America, and is located in the Pacific Ring of Fire, one of the world's most active seismic areas. Station designs incorporated the last innovations in the Earthquake Engineering field, as the most recent developments in seismicity, dynamic behavior of materials and soil-structure interaction. An optimal, reliable, robust and safe design was achieved, which arouse satisfaction in all the different entities involved in the project.

KEYWORDS: Earthquakes, Numerical Modeling, Seismic Design, Soil-Structure Interaction

1. Introduction

L2 Metro Lima is the largest underground train project under construction in Latin America. Construction is in charge of CJV (FCC-Dragados-Impregilo-COSAPI), and AYESA Engineering and Architecture plays the designer role for the stations.

City of Lima is situated in one of the world's most hostile tectonic environment, the Pacific Ring of Fire, where large earthquakes occur on a regular basis. Seismic conditions are then of capital importance for the project during both design and construction process.

Underground structures provide the necessary infrastructure for many services and facilities in modern cities. In the majority of cases they are expensive and difficult to build. Additionally, their failure might often compromise other aboveground structures in their vicinities. For these reasons they should be designed to resist severe seismic events if they are located in cities like Lima. Stochastic processes that govern seismic events and dynamic behavior of buried structures make their design process a very complex, challenging task that is still unsolved nowadays.

Several simplified approaches are used in practical engineering for design of underground structures. Those might be divided into two main groups: force-based and deformation-based methods.

Force-based methods simplify the seismic action as a static pressure on the wall that results in the same maximum forces than those achieved during the earthquake event. Examples of this method are shown in [1]. This method assumes dynamic thrust to be an inertial force applied to the structure. This condition mainly applies for cantilever walls, so it might not be properly applied for design of underground structures.

Displacement-based methods simplify the seismic action as the maximum drift of the buried structure which will take place during the earthquake. Examples of this methods can be found in [2]. This method assumes the seismic action to have a horizontal swing effect only (racking), and thus displacement-based design is useful for box-like shaped structures, like cut-and-cover tunnels. Nevertheless, author states that underground structures may behave in a more complicated way that cannot be approximated by this method.

The structural system of the Mercado Santa Anita station is composed by column-piles, which sustain the gravity loading of the roof and the slabs, and by retaining walls, which resist lateral forces coming from earth pressures and earthquake excitation. Then, they do not comply hypothesis of displacement-based methods.

Both force and displacement-based methods were shown to poorly predict behavior of simple-shaped buried structures, as in [3]. The authors show that a more reliable approach is needed for seismic design of underground structures. They also recommend full-time history dynamic analysis as the most accurate method for seismic design, according to laboratory tests data.

This approach was adopted for the seismic design of L2 Metro Lima. Current state-of-the-art and latest innovations were applied to the project, as stated in [4] and [5], and also in cooperation with the University of California Berkeley. This approach was successfully used to develop an optimal, reliable, robust and safe design, with great satisfaction of both contractor and administration.

2. Methods

First, seismic design scenarios were determined through a probabilistic seismic hazard analysis (PSHA). Then, geotechnical model of the site was elaborated based on available tests and bibliographical data. Shear wave velocity (Vs) profile was used to compute the input seismic signal for the numerical model. Both geotechnical and structural models were implemented in finite element software PLAXIS2D. Mesh and boundary conditions were especially treated in order to develop an accurate dynamic numerical model. Finally, dynamic calculations were performed, and obtained results were utilized to feed the structural design process.

2.1. Determination of design seismic scenarios

PSHA is the most proper method to determine the different scenarios for seismic design [6]. PSHA allows the designer to quantify all uncertainties that are inherent to the process of seismic design scenario determination through the definition of the different involved stochastic variables.

The main variables that have been used to determine the level of seismic excitation are moment magnitude M_w, distance to fault rupture R, failure mechanism F and shear wave velocity of the upper $30\ m$ of soil V_{30}.

Two different scenarios were chosen, which were called Operational Basis Earthquake (OBE) and Maximum Conceivable Earthquake (MCE). The structure should be fully operational after the first

scenario takes places, while repairable damage is allowed for the second. It was arranged with the client that OBE corresponds to a return period of $1000\,y$, and MCE to $2500\,y$.

Historical site seismicity of Lima was studied in order to determine a Gutenberg-Richter law [6]. M_w for OBE and MCE scenarios were computed, given 8.9 and 9, respectively. R_D was assumed to be equal to the distance to the nearest active fault for all cases due to the lack of information. This distance was measured as about $40\,k$. Fault rupture type was chosen as subduction intraplate because of the local tectonic environment. V_{S30} was determined from the *in situ* shear wave velocity tests carried out in the station area. A value of $550\,m/s$ was obtained.

Target response spectra for each scenario were obtained through usual ground motion prediction equations (GMPE), as in [4], with unit weight factors for the applicable GMPEs. Mean plus half standard deviation was used for calculation of target response spectra, for the sake of safety. Those response spectra are the expected maximum seismic demand at surface, in terms of accelerations, that the earthquake associated to each scenario will induce to the soil-structure system.

2.2. Elaboration of the geotechnical model

A large number of in situ and laboratory tests were carried out in the area of Mercado Santa Anita station. The aim of the tests was the geotechnical characterization of the site, and especially the development of its V_S velocity profile.

Lima is founded on a very thick gravel deposit which was formed by the Rimac river floods. Depth to rock was unknown for Mercado Santa Anita site, since bedrock was not found in any of the soundings nor the shear wave velocity tests. Water table was not found either in the area for a depth above $60\,m$. This soil is very stiff and strong, and can sustain slopes up to $82°$. Soil was classified as poorly-graded gravel GP. Mean uniformity coefficient (U_C) was computed as 166, with average grain size of $30\,m$. Large boulders were found in samples. Low fine content with low plasticity was observed. Unit weight ranged between $20\,k$ $/m^3$ and $22\,k$ $/m^3$. An anthropic fill R with low resistance and stiffness was found over the gravel deposit. Several layers of silty sand SM were reached with boreholes. Those layers are weaker than the gravel deposits.

It was decided to divide the gravel deposit into three different layers. They correspond to the different degree of compactness, which affects the V_S . Then, GP-Ss, GP-Sm and GP-Sf were differentiated for gravels with $V_S < 400\,m/s$, $V_S < 600\,m/s$ and $V_S > 600\,m/s$ respectively.

Shear strength parameters for cohesion c and friction angle φ of the different soils were obtained from laboratory tests and from in-situ large-scale direct shear tests. Different shear strength parameters were given to R, GP-Ss, GP-Sm, GP-Sf and SM. Tensile strength was taken as $\sigma_t = {}^{c}/_{\tan\varphi}$. Dilatancy cut-off was accounted for by choosing a parameter $\delta = 0.09$ for soils with positive dilatancy angle, as recommended by [7].

Hardening Soil with Small-strain Stiffness model (HSsmall) was selected as the constitutive model to simulate soil behavior. This was done since HSsmall can accurately predict both the static and dynamic behavior of soils, and also the hysteretic damping that strain cycles trigger.

HSsmall relates shear stiffness to minor confining pressure σ_3 and plastic parameters c and Φ as:

$$G_0 = G_0^{r} \left(\frac{\sigma_3 \cdot s \Phi + c \cdot \cos\Phi}{100\,k \cdot s \Phi + c \cdot \cos\Phi} \right)^{m} \quad (1)$$

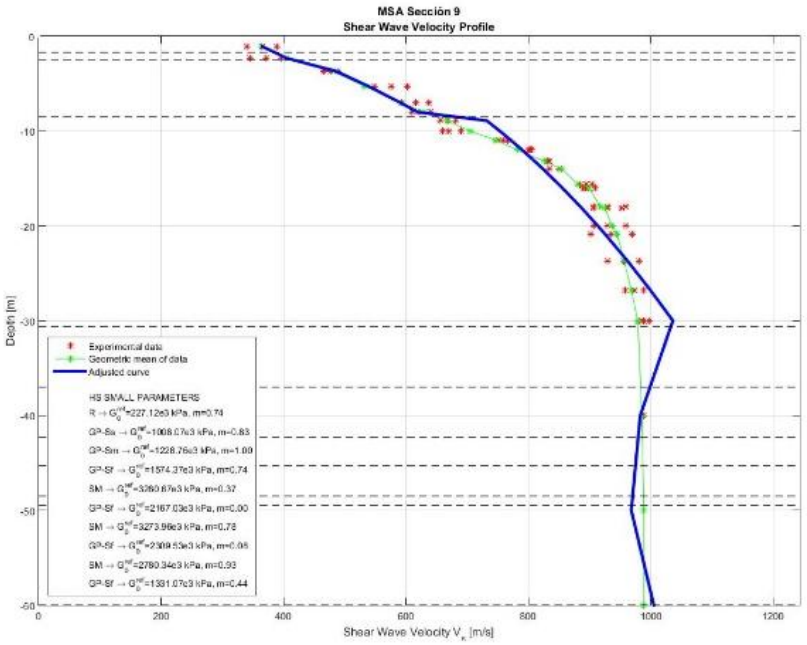

Figure 1. Shear wave velocity profile fitting.

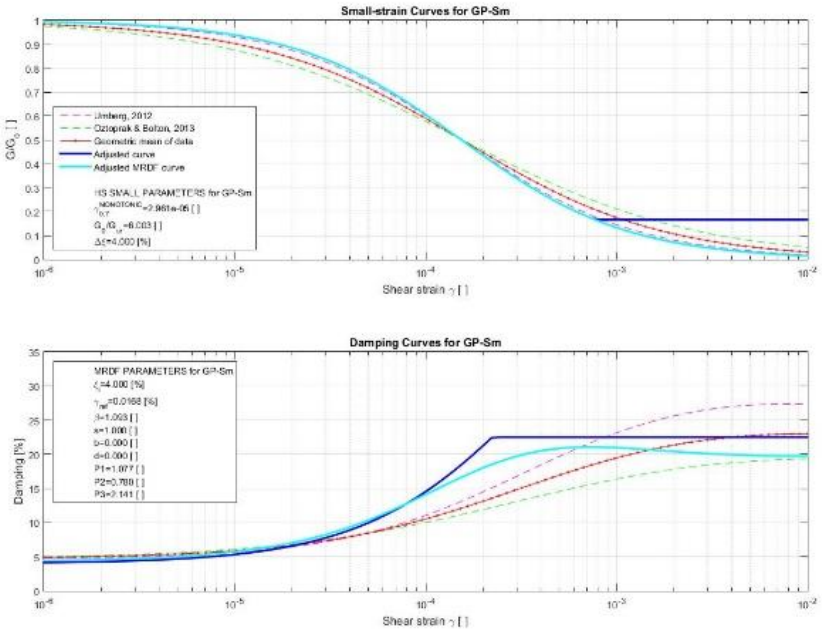

Figure 2. SM1 stiffness reduction curve fitting (right)

Stiffness parameters were based on the results of the shear wave velocity tests and on bibliographical data. Small-strain shear modulus was directly computed from the V . An optimization procedure was coded to determine the parameters G_0^r and m for each layer that provided the best fit to the mean of the V measured in the field for each depth.

PLAXIS implements the stiffness degradation curves following the formulation in [7]. Stiffness degradation curves for the different layers were computed to best-fit the mean from [8] and [9] utilizing formulation implemented in PLAXIS. An optimization procedure was coded in order to obtain the parameter $\gamma_{0.7}$, and also the value of damping at small strains for the soil for each different layer differentiated in the soil profile. U was limited to $U = 100$, since authors of the used formulations do not recommend to use higher values due to database limitations.

Damping at small strains was introduced as Rayleigh damping. Value of damping came from the fitting process, and period range was chosen as $0.2 \cdot T - 2.0 \cdot T$, where T is the natural period of the soil deposit, in accordance with [5]. For Mercado Santa Anita, it was found that $T = 0.40\ s$.

Layer	Top [m]	Bot. [m]	γ [kN/m³]	e [ ]	e_{min} [ ]	e_{max} [ ]	α [ ]	β [ ]	c [kPa]	Φ [°]	Ψ [°]
R	0	1.7	16.7	0.56	0.25	0.75	0.4571	3.92E-04	1	28	0
GP-Ss	1.7	2.5	20	0.19	0.15	0.25	1.1468	9.83E-04	15	34	2
GP-Sm	2.5	8.5	21	0.19	0.15	0.25	1.1468	9.83E-04	27.5	36.5	4.5
GP-Sf1	8.5	30.6	22	0.19	0.15	0.25	1.1075	9.49E-04	40	39	7
SM1	30.6	37	16.95	0.56	0.25	0.75	0.2041	1.75E-04	5	30	0
GP-Sf2	37	42.3	22	0.19	0.15	0.25	0.9745	8.35E-04	40	39	7
SM2	42.3	45.3	16.95	0.56	0.25	0.75	0.1946	1.67E-04	5	30	0
GP-Sf3	45.3	48.5	22	0.19	0.15	0.25	0.9446	8.10E-04	40	39	7
SM3	48.5	49.5	16.95	0.56	0.25	0.75	0.1906	1.63E-04	5	30	0
GP-Sf4	49.5	60	22	0.19	0.15	0.25	0.9168	7.86E-04	40	39	7

Table 1. State, strenght and small-strain damping parameters of soils used for analysis in PLAXIS.

Layer	Top [m]	Bot. [m]	E_{50}^{ref} [kPa]	E_{oed}^{ref} [kPa]	E_{ur}^{ref} [kPa]	m [ ]	$\gamma_{0.7}$ [ ]	G_0^{ref} [kPa]
R	0	1.7	30283	30283	90848	0.74	2.59E-05	227120
GP-Ss	1.7	2.5	134413	134413	403240	0.83	2.45E-05	1008100
GP-Sm	2.5	8.5	163840	163840	491520	1.00	2.96E-05	1228800
GP-Sf1	8.5	30.6	209920	209920	629760	0.74	4.00E-05	1574400
SM1	30.6	37	437427	437427	1312280	0.37	1.73E-04	3280700
GP-Sf2	37	42.3	288933	288933	866800	0.00	4.87E-05	2167000
SM2	42.3	45.3	436533	436533	1309600	0.78	2.00E-04	3274000
GP-Sf3	45.3	48.5	307933	307933	923800	0.08	5.19E-05	2309500
SM3	48.5	49.5	370707	370707	1112120	0.93	2.13E-04	2780300
GP-Sf4	49.5	60	177480	177480	532440	0.44	5.50E-05	1331100

Table 2. Stiffness parameters of soils used for analysis in PLAXIS.

2.3. Determination of design acceleration time series

In order to perform a full-time history analysis with a numerical model, an acceleration time series is required. This accelerogram is normally applied to the base of the numerical model as an input.

Acceleration time series for both seismic scenarios should be such that they result in a peak spectral acceleration (PSA) at surface that is equal to target spectrum. Seismic records do not provide the target response spectra as PSA at surface on a regular basis, so they should be modified, through a process called spectral matching [10], in order to fulfill that condition.

Then, a certain seismic record, called seed ground motion, is spectrally-matched to make its PSA to be equal to the target spectrum. This modified record is the expected earthquake excitation at surface for a certain seismic scenario.

Spectral matching process was undertaken according to [5]. First, Maule Earthquake (Chile, 2011) record at Puente Alto was used as the seed ground motion. This was done because it corresponds to an earthquake with similar characteristics to that expected in Lima for the OBE seismic scenario: a subduction intraplate earthquake, with $M_w = 8.4$, $R_D \sim 80\ k$ and $V \sim 450\ m/s$. Additionally, PSA of Maule Puente Alto record is similar in shape to the target spectrum, which makes the matching

process easier. Also, it is an earthquake that took place in the same tectonic area as Lima, so local seismicity was implicitly implemented with the selection of the seed ground motion.

Then, a spectrally-matched ground motion was obtained for each seismic scenario, which correspond to excitation at surface. For numerical modeling purposes, an input ground motion is needed at the base of the model. This should result, after site amplification, in the spectrally-matched ground motion for each scenario.

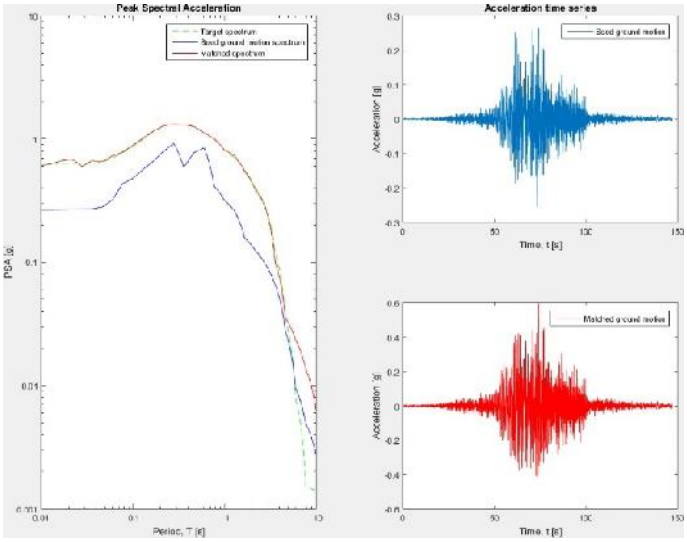

Figure 3. Spectrally-matched ground motion for MCE

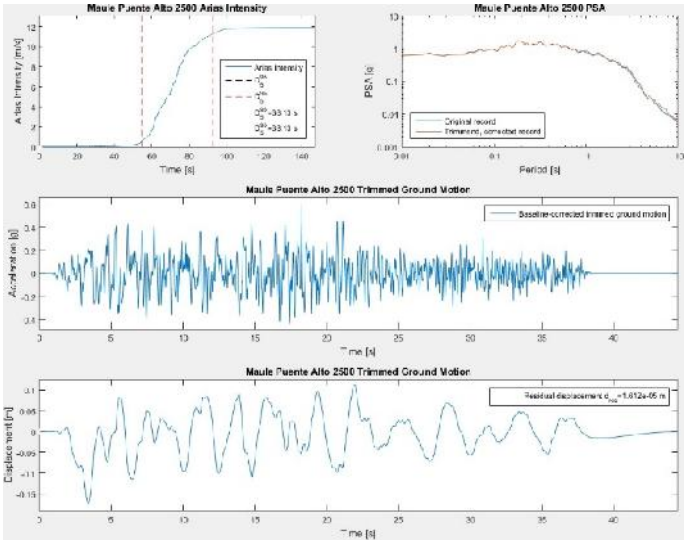

Figure 4. Trimmed ground motion for MCE scenario.

The input ground motions were obtained by means of the deconvolution process. A linear equivalent analysis was performed through wave propagation software DEEPSOIL [11], given a site profile and a surface ground motion, to obtain the seismic excitation at the base of the model, called deconvolved ground motions. Fitted MRDF parameters were used in the software. A within motion was assumed for deconvolution. Thus, deconvolved ground motions are those that will propagate from the bottom of the model to the top resulting in the spectrally-matched ground motion for each seismic scenario.

Deconvolution process assumes equivalent linear behavior of the soil. This means that no plastic deformations will occur during the seismic excitation. While this is true, upward propagation of the deconvolved ground motion will provide the associated spectrally-matched motion. If plastic deformation takes place, as in large earthquakes or weak soil, propagated ground motion will differ from the spectrally-matched motion. Nevertheless, the differences will be significant only in period ranges that are much shorter and much larger than that of the soil-structure system. Then, seismic demand on the system will be accurately computed regardless of the existence of plastic behavior, and design of structural members could be adequately performed.

In order to reduce computational effort, a trimming and filtering procedure was specifically developed for this project. Motion was trimmed to its significant duration, which is the time comprised between the one at which 5% and 95% of Arias intensity are achieved. Then, a recursive high-pass Butterworth filter with corner frequency of $0.1\,H$ was applied to baseline-correct the trimmed motion.

2.4. Elaboration of structural model

Mercado Santa Anita Station was thought to be a 150mx30m retaining wall-supported pit. 12 rows of two 10m-to-15m spaced pile-columns will support the slabs. Three slabs were designed, which correspond the ceiling, the hall floor and the station bottom, which provide restraint for the horizontal forces on retaining walls, mainly coming from earth pressures and seismic actions. The pile-columns withstand the major part of the vertical loads. Also, lateral deflections due to earthquake will pose some additional forces on them that should be taken into account for design.

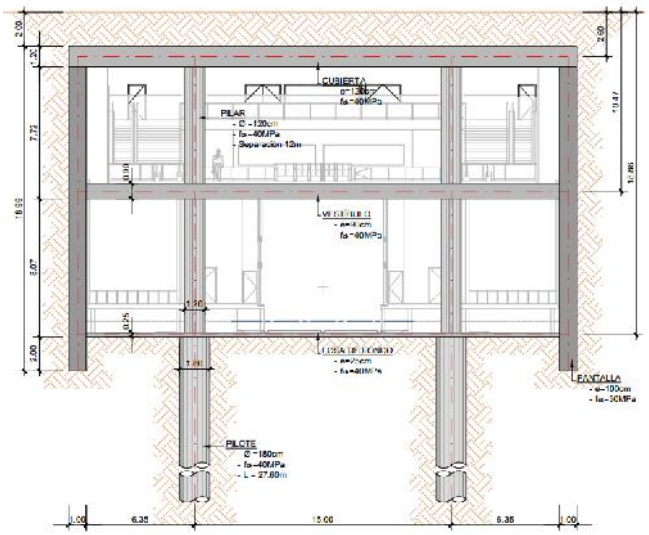

Figure 5. S09 section. [fck=40MPa for all elements except for the 100cm-thick retaining walls -fck=30MPa- , -fyk=420MPa-. Thickness of slabs are 120cm for ceiling, 90cm for the hall and 25 cm for the bottom slab. Columns and piles are 120cm and 180cm respectively].

Section which design is presented is called S09, and is shown in ***Figure 5***.

For the piles, embedded beam row elements in PLAXIS were used. They simulate the behavior of a row of structural elements with skin friction and end bearing resistance located at a certain spacing. For the walls, plate elements in PLAXIS were used. They model the behavior of continuous structural elements with an interface that simulates the reduction of soil stiffness and strength in close contact with it.

Structural properties of these elements were computed depending on the geometry of its members for OBE scenario. Reinforcing steel for walls was designed with structural forces computed for that case, and moment-curvature (M-k) diagrams were calculated for each different reinforcing section of each wall. Those M-k diagrams were implemented in PLAXIS for MCE scenario. An example is shown in ***Figure 9***.

Retaining walls reinforcement was designed to behave elastically for OBE conditions. For MCE the structural capacity of the walls was checked utilizing a nonlinear elastoplastic behavior through moment-curvature diagrams. Sufficient shear strength was provided during design.

Since about 90% of the gravity loads are taken by the columns-pile system, they were designed to remain elastic for both OBE and MCE scenarios.

Skin friction and end bearing resistance of piles were obtained by averaging recommendations in [12] and [13]. Interface property $R_{ti} = 0.8$ was assumed, since wall is not allowed to deflect significantly because slabs are cast-in-place before deeper excavation is started.

All connections between elements were simulated as joints which allowed connecting members to rotate independently. “Consider gap closure” option was activated for all plate elements, so that soil does did not immediately contact the plate when stress reversals happen if a gap develops.

2.5. Mesh and boundary conditions

Mesh conditions are important for dynamic analysis, since elements size should fulfill different criteria in order to accurately simulate the propagation of seismic waves into the model.

First, aliasing had to be avoided, according to [7]. Aliasing is a phenomenon that consists in the loss of information produced by the insufficient sampling rate with respect to the wave frequency. A number of nodes per element of 15 was chosen in order to increase maximum element size, for the sake of velocity in calculations. The maximum frequency of interest for the analysis was set to $10\,H$, since higher frequencies do not contribute to seismic response of soil-structure system in a significant manner.

Second, calculation time step had to be properly determined. Conditions in [7] should be fulfilled in order to guarantee the stability of the dynamic analysis. For every soil element, with a certain V_s and v, which refer to the Poisson's ratio in its cyclic behavior, there is a maximum allowable time step [7]. Since V_s will vary during seismic excitation, $\Delta t = 0.002\,s$ was taken, which corresponds to the mean of both of Δt computed for small-strain and large-strain conditions.

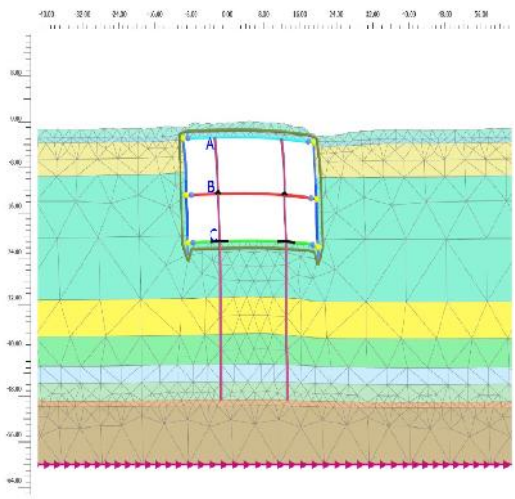

Figure 6. Deformed shape of the model.

Boundary conditions are also crucial for dynamic analysis. First, the station is located at the center of the model, which depth is about three times the maximum depth of the walls (i.e. $60\,m$). The width of the model was taken as 2.5 times its depth, according to [14]. "None" condition in PLAXIS, also called "rigid base", was selected for the base of the model, since "within motion" condition was taken for deconvolution. "Tied degrees of freedom" was chosen for the lateral boundaries, since it allows to compute free-field motion without boundary reflection effects. Mesh was forced to be symmetric at the lateral boundaries in order to be able to apply this condition.

Deconvolved motion for each seismic scenario was applied at the bottom of the model. A line displacement was created at that location, and an acceleration multiplier, with acceleration values at all times, was applied. "Drift correction" option was allowed in order to force PLAXIS to avoid residual velocities and displacements in the model.

3. Results and discussion

3.1. Validation of dynamic numerical model

Deconvolved motion should propagate to surface to achieve target response spectrum at that location. Then, validation of the numerical model can be performed by comparison of target response spectrum and spectrum at surface obtained by means of PLAXIS.

Natural period of soil deposit was computed to be 0.40 s. It can be checked in *Figure 7* that, for periods ranging between $T = 0.2\,s - 2\,s$, which envelope the natural period of soil profile, PLAXIS spectrum accurately matches target spectrum. This proofs that the numerical model was properly developed, and leads to the conclusion that it propagates shear waves in an accurate way.

Then, forces on structural members that were computed represent those that will develop when seismic excitation reaches the two scenarios that were studied.

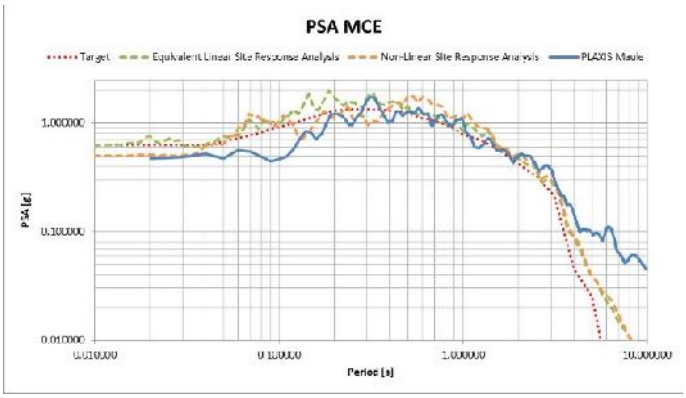

Figure 7. PSA comparison for and MCE scenario

3.2. Results for OBE and MCE scenarios

Forces envelope and capacity for the retaining walls of S09 in OBE and MCE conditions are shown in *Figure 8*.

Several models of the station with different material behavior of the retaining walls were analyzed in order to perform MCE scenario checks. Considered behaviors were elastic (E-I) and elastic-perfectly plastic (M-p), which were used to predict the location of plastic hinges, and nonlinear elastoplastic (M-k), which was employed to check reinforcement capacity. Results for each model are shown in *Figure 8*. It can be seen that, for S-c, moment and shear capacity was exceeded, and a plastic hinged could develop. Shear strength had to be increased in order to avoid brittle failures.

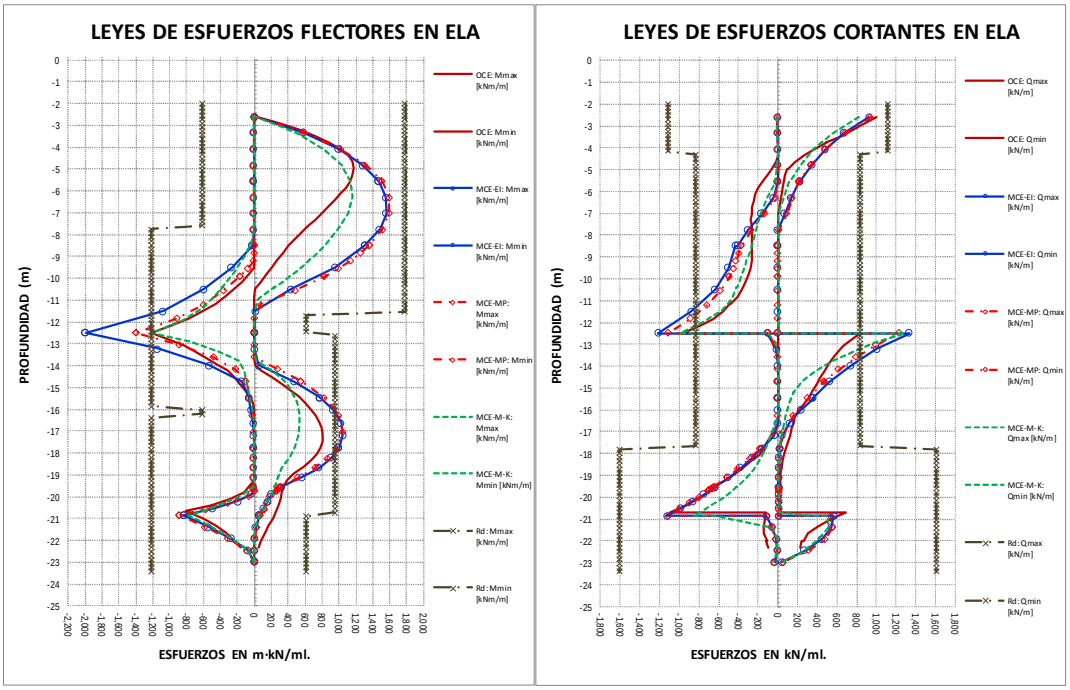

Figure 8. Forces envelopes for OBE and MCE versus capacity.

Performance of the potential plastic hinge at S-c was checked with MCE forces for M-k model. When earthquake ceases, forces will return to those of the static conditions. Maximum bending moment at S-c for static and MCE were found as $M_M = 1218\, m \cdot k$ and $M_M = 300\, m \cdot k$.

It was checked that reinforcement reaches plastic behavior with elongation lower than 0.2%, so performance point lays in Security Level III, according to [15]. Maximum forces for column-piles obtained for the different design scenarios in *Table 3* show that ULS results are close to those of the MCE scenario, because of the partial factors that are disregarded in seismic calculations. [13].

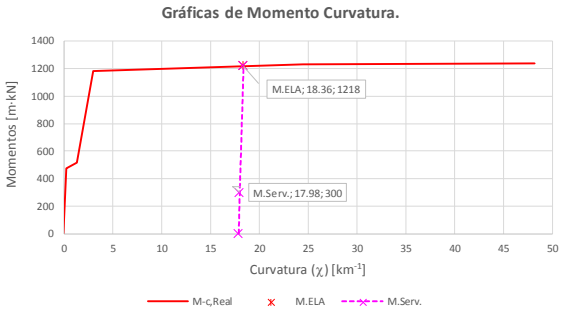

Figure 9. Performance point of S-c in MCE

		(N,M) [kN,m·kN]	Efficiency [%]
ULS	Column	(29090,3279)	99
	Pile	(69959,3534)	52
OBE	Column	(22316,4100)	74
	Pile	(6350,4132)	25
MCE	Column	(23212,5720)	99
	Pile	(7050,6120)	52

Table 3. Forces on column-piles

4. Conclusions

The methodology described in this article was successfully applied to perform an optimal, reliable, robust and safe design of the structural elements in the station Mercado Santa Anita, in L2 Metro Lima. This arouse satisfaction in all the different entities involved in the project.

In the authors' opinion, the methodology developed for the project will become the state-of-practice for seismic design of underground structure for the coming years.

References

[1] Geraili Mikola, R., & Sitar, N. (2012). Seismic earth pressures on retaining structures in cohesionless soils. Report UCB GT 13-01. PEER

[2] Wang, J.-N. (1993). Seismic Design of Tunnels, 1991 Parsons Brinckerhoff Monograph 7, (1993).

[3] Tsinidis, G., Pitilakis, K., Madabhushi, G., & Heron, C. (2015). Dynamic response of flexible square tunnels : centrifuge testing and validation of existing design methodologies. Géotechnique, (5), 401–417.

[4] Carlton, B. D., Pestana, J. M., & Bray, J. D. (2015). Selection of target ground motion parameters for nonlinear site response analysis, GeoEngineering Report UCB/GE/2015-01, PEER

[5] Carlton, B. D., Pestana, J. M., & Bray, J. D. (2015). Selection of ground motion time histories for nonlinear site response analysis, GeoEngineering Report UCB/GE/2015-02, PEER

[6] Baker, J.W., An Introduction to Probabilistic Seismic Hazard Analysis (PSHA), Stanford University Press, October 2008

[7] Brinkgreve, R. et al. (2016) PLAXIS2D, PLAXIS bv, TU Delft.

[8] Oztoprak, S., & Bolton, M. D. (2013). Stiffness of sands through a laboratory test database. Géotechnique.

[9] Umberg, D. (2012). Dynamic properties of soils with non-plastic fines. University of Texas at Austin.

[10] Alatik, L., & Abrahamson, N. (2010). An improved method for nonstationary spectral matching. Earthquake Spectra, 26(3), 601–617. http://doi.org/10.1193/1.3459159

[11] Hashash, Y. et al. (2002-2016) DEEPSOIL, 1-D wave propagation analysis program for geotechnical site response analysis of deep soil deposits, Board of Trustees of University of Illinois at Urbana-Champaign

[12] AASHTO LRFD Bridge Design (2012)

[13] EN 1997-1 (2004)

[14] Amorosi, A., Boldini, D., & Elia, G. (2010). Parametric study on seismic ground response by finite element modelling. Computers and Geotechnics, 37(4), 515–528.

[15] FEMA 365